Optical Engineering

OpticalEngineering.SPIEDigitalLibrary.org

Absolute phase unwrapping for dual-camera system without embedding statistical features

Chufan Jiang
Song Zhang

SPIE.

Chufan Jiang, Song Zhang, "Absolute phase unwrapping for dual-camera system without embedding statistical features," *Opt. Eng.* **56**(9), 094114 (2017), doi: 10.1117/1.OE.56.9.094114.

Absolute phase unwrapping for dual-camera system without embedding statistical features

Chufan Jiang and Song Zhang*
Purdue University, School of Mechanical Engineering, West Lafayette, Indiana, United States

Abstract. This paper proposes an absolute phase unwrapping method for three-dimensional measurement that uses two cameras and one projector. On the left camera image, each pixel has one wrapped phase value, which corresponds to multiple projector candidates with different absolute phase values. We use the geometric relationship of the system to map projector candidates into the right camera candidates. By applying a series of candidate rejection criteria, a unique correspondence pair between two camera images can be determined. Then, the absolute phase is obtained by tracing the correspondence point back to the projector space. Experimental results demonstrate that the proposed absolute phase unwrapping algorithm can successfully work on both complex geometry and multiple isolated objects measurement. © *2017 Society of Photo-Optical Instrumentation Engineers (SPIE)* [DOI: 10.1117/1.OE.56.9.094114]

Keywords: phase unwrapping; fringe projection; phase shifting; epipolar geometry; stereo matching.

Paper 170730P received May 12, 2017; accepted for publication Sep. 12, 2017; published online Sep. 28, 2017.

1 Introduction

High-speed optical three-dimensional (3-D) shape measurement has been widely adopted in many applications ranging from online inspection to disease diagnosis.[1] Among optical 3-D shape measurement techniques, phase-shifting-based methods are advantageous because of their high measurement speed, high measurement accuracy, and robustness to noise or surface reflectivity variations.[2]

For phase-based 3-D shape measurement technologies, phase unwrapping has always been a crucial step for correctly reconstructing 3-D geometry and at the same time a challenging problem. Existing phase unwrapping algorithms are generally divided into two categories: spatial and temporal phase unwrapping. Spatial unwrapping algorithms[3] unwrap phase by referring to other pixels on the same phase map. The unwrapping result depends on the obtained phase quality and, thus, is sensitive to the existence of noise. One of the most robust methods is creating a quality map to guide the unwrapping path such that pixels with higher phase quality will be unwrapped earlier than those with lower phase quality.[4] In general, spatial phase unwrapping only produces relative phase maps. Moreover, the assumption that the phase is locally smooth makes it inapplicable for measurement of surfaces with abrupt depth changes or on multiple isolated objects.

Temporal phase unwrapping algorithms, on the other hand, encode the absolute phase value into specific patterns and retrieve the fringe order, the number of 2π's to be added for each point, by analyzing additionally acquired information at a temporally different time. The absolute phase map is obtained since the fringe order is determined by acquiring additional information rather than referring to the phase value of other points. Conventional temporal unwrapping methods that originated from laser interferometry include two to multiwavelength phase-shifting algorithms.[5,6] In a digital fringe projection (DFP) system, encoded patterns can be designed in many ways besides sinusoidal patterns, such as a sequence of binary patterns,[7] a single statistical pattern,[8] a single stair image,[9] etc.

Although working robustly on single-camera and single-projector DFP systems, temporal phase unwrapping is not desirable for high-speed applications since additional patterns acquisition slows down the measurement speed. Currently, with the reduced cost and improved performance of hardware, researchers have developed alternative absolute phase unwrapping methods by adding a second camera to the system, which is often referred to as the multiview method. This multiview system is over-constrained by obtaining more restrictions from different perspectives, which makes it possible for absolute phase retrieval without temporally acquiring additional patterns. Because two cameras are involved, a standard stereo-vision approach is naturally introduced to determine correspondence points between two cameras and to offer additional conditions for phase unwrapping. It is widely known that passive stereo can easily fail on low texture surfaces; consequently, the projector projects other structured patterns (e.g., random dots,[10] band-limited random patterns,[11] binary-coded patterns,[12] color structured patterns,[13] or phase-shifted sinusoidal fringe patterns[14]) to actively add surface features on an object and use it for a unique correspondence determination.

The aforementioned phase unwrapping methods require at least one additional image capture for absolute phase retrieval. To achieve a maximum measurement speed, multiview geometric constraints-based absolute phase unwrapping methods have been recently developed. Instead of projecting more patterns, the geometric relationships among system components are employed to obtain more information. A variety of constraints (e.g., wrapped phase, epipolar geometry, measurement volume, phase monotonicity, etc.) are applied to limit the number of candidates for absolute

*Address all correspondence to: Song Zhang, E-mail: szhang15@purdue.edu

phase determination.[15–22] Ishiyama et al.[18] proposed finding the closest wrapped phase value for matching points searching. Although easy to implement, a unique correspondence cannot always be guaranteed. Bräuer-Burchardt et al.[15] enhanced the chance of correct correspondence by applying phase monotonicity constraints along an epipolar line after determining reference points. Because a backward and forward checking is required to finally select the correct corresponding point out of all candidates, the computation speed is slow. A sequence of studies[19–21] found correspondence on phase maps using the trifocal tensor to reject candidates through a mixture of volume constraints, stereo-view disparity range, and intensity difference. These algorithms achieve satisfying robustness on arbitrary shape measurement, but they are sensitive to phase error, and a time-consuming refinement process is required for phase error reduction and correspondence coordinate correction. An alternative approach is to speed up the searching process by embedding a statistically unique structured pattern along with the fringe pattern for unique correspondence determination.[23,24] While this approach works well on correspondence matching, the phase quality is sacrificed due to the embedded statistical pattern into the fringe pattern.

This paper proposes an absolute phase unwrapping algorithm that addresses these problems from two camera approaches. The first step is to calibrate all three devices: both cameras and the projector. Then for each left camera pixel, multiple right camera candidates are generated from the system geometric relationship. Given all candidate rejection constraints, the final correspondence pair associated with a projector phase line can be obtained for phase unwrapping. Experimental results are provided to demonstrate the success of the proposed method.

Section 2 explains the principle of the proposed method. Section 3 shows experimental data, and finally Sec. 4 summarizes this paper.

2 Principle

Figure 1 shows the computational framework of the proposed multiview geometric constraints-based phase unwrapping approach. Essentially, we utilize additional geometric constraints provided by the second camera to retrieve the absolute phase. For any pixel on the left camera, its wrapped phase ϕ_0 corresponds to a finite number of phase lines on the projector. An epipolar line is introduced here to limit the range of potential projector candidates. Once the projector and left camera are calibrated under the same world coordinate, 3-D coordinates (x^w, y^w, z^w) of each projector candidate can be reconstructed. Then, a predefined measurement volume constraint is used to further reduce the number of candidates. If the right camera and the projector are also calibrated in the same world coordinate, all 3-D points within the volume of interest can be projected on the right camera image. With employment of various candidate rejection algorithms, a final correspondence is determined, and we can trace it back to the projector space to obtain the absolute phase value.

2.1 *Least-Squares Phase-Shifting Algorithm*

Phase-shifting algorithms are widely used in 3-D optical measurement because of their high speed and high accuracy.[2] Various phase-shifting algorithms have been developed for different application needs, such as measurement speed, measurement accuracy, or sensitivity to disturbance. Typically, using phase shifted patterns with more steps achieves better phase quality. For an N-step phase-shifting algorithm[25] with equal phase shifts, the k'th fringe image can be mathematically represented as

$$I_k(x,y) = I'(x,y) + I''(x,y)\cos(\phi + 2k\pi/N), \tag{1}$$

where $\delta_k = 2k\pi/N$ is the phase shift and $\phi(x,y)$ is the phase to be solved.

Simultaneously, solving these N equations in a least squares manner leads to

$$\phi(x,y) = -\tan^{-1}\left[\frac{\sum_{k=1}^{N} I_k \sin(2k\pi/N)}{\sum_{k=1}^{N} I_k \cos(2k\pi/N)}\right]. \tag{2}$$

The calculated phase value $\phi(x,y)$ is wrapped within the $(-\pi,\pi]$ interval with 2π discontinuities. The real phase $\Phi(x,y)$ should be a continuous function of $\phi(x,y)$ by adding or subtracting an integer number of 2π

$$\Phi(x,y) = \phi(x,y) + 2\pi k(x,y). \tag{3}$$

The integer number $k(x,y)$ is called the fringe order, and this process is called phase unwrapping. If fringe order $k(x,y)$ can be uniquely determined and is consistent with a predefined value in projector space, the unwrapped phase is called absolute phase.

2.2 *Projector Candidate Selection*

For a left camera pixel with a wrapped phase value calculated from the phase-shifting algorithm, we can "guess" its unwrapped phase by assigning different values for the fringe order $k(x,y)$ in Eq. (3). There is only a finite number of possible fringe orders in the projector image domain, and each of them corresponds to one absolute phase line. As long as the correct phase line is calculated, the phase value of the line is the unwrapped absolute phase on this pixel.

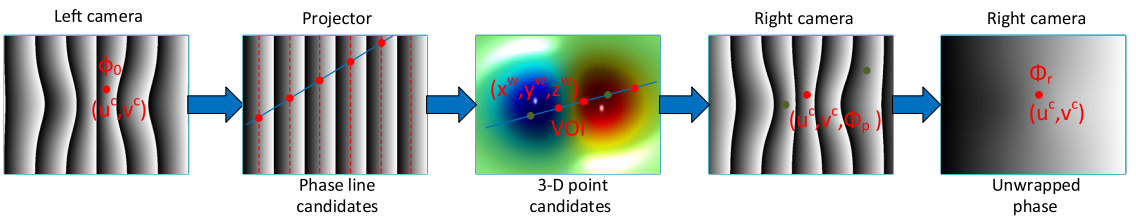

Fig. 1 Framework of the proposed multiview geometry-based absolute phase unwrapping.

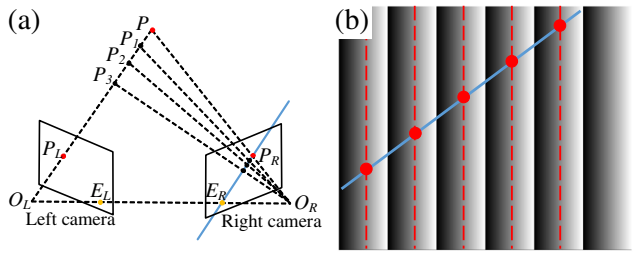

Fig. 2 Projector candidate selection. (a) Illustrative diagram of epipolar geometry and (b) schematic of projector candidate decision.

To reduce the number of candidates, epipolar geometry[26] is exploited to confine the range of projector mapping points. Epipolar geometry describes geometric constraints on the correspondence relationship between two imaging devices. Figure 2(a) shows a schematic diagram of the stereo vision system with two cameras capturing images from different perspectives. For each camera, all light rays converge to the focal points O_L or O_R of the lens. Given a pixel P_L on the left camera image, all 3-D points that could project on P_L lie on a ray along $\overline{O_L P_L}$. When these 3-D points are captured by the right camera, they are also projected into a line called the epipolar line (blue line). Connecting imaging point P_L with two camera focal points O_L and O_R forms a plane called the epipolar plane. In fact, the intersection line $\overline{E_R P_R}$ between the epipolar plane and the right camera imaging plane is the epipolar line.

In a conventional structured light system, the right camera is substituted by a projector, but epipolar constraints are still established. For a given pixel from the left camera, only pixels along the epipolar line could be potential projector candidates, which restricts the searching range. Combined with the wrapped phase value of this pixel, we can select projector candidates as shown in Fig. 2(b). The solid blue line is the epipolar line from the system geometric relationship, the red dashed lines are phase lines corresponding to the wrapped phase, and the red intersection points are decided projector candidates.

2.3 *Right Camera Candidate Projection*

Once projector candidates are decided, we map them onto the right camera image plane, so we can use image information between two cameras to find the true correspondence. Figure 3(a) shows a diagram of the multiview system including two cameras and one projector. For each projector candidate (u^p, v^p), we first reconstruct the corresponding 3-D point (x^w, y^w, z^w) based on the triangulation relationship between the left camera and projector. Then, this 3-D point in the world coordinate is projected on a two-dimensional (2-D) image plane of the right camera, denoted as the point (u^{c2}, v^{c2}).

Both reconstruction and projection are based on a well-known pinhole model since a nontelecentric lens is used.[27] Figure 3(b) shows the schematic of the imaging system that models the projection from 3-D world coordinate to 2-D imaging plane. Mathematically, this projection can be described as

$$s[u, v, 1]^{\mathrm{T}} = A[R, t][x^w, y^w, z^w, 1]^{\mathrm{T}}, \tag{4}$$

where s is the scaling factor, $[u, v, 1]^{\mathrm{T}}$ represents the homogeneous image coordinate on the imaging plane, and $[R, t]$ denotes the extrinsic parameters

$$R = \begin{bmatrix} r_{11} & r_{12} & r_{13} \\ r_{21} & r_{22} & r_{23} \\ r_{31} & r_{32} & r_{33} \end{bmatrix}, \qquad t = \begin{bmatrix} t_1 \\ t_2 \\ t_3 \end{bmatrix}. \tag{5}$$

The extrinsic parameters describe the transformation relationship from the 3-D world coordinate (x^w, y^w, z^w) to the camera lens coordinate (x^c, y^c, z^c) by a 3×3 rotation matrix R and a 3×1 translation vector t. The projection from the lens coordinate to the 2-D imaging plane is modeled through the intrinsic matrix A

$$A = \begin{bmatrix} \alpha & \gamma & u_0 \\ 0 & \beta & v_0 \\ 0 & 0 & 1 \end{bmatrix}, \tag{6}$$

where α and β are the effective focal lengths along the u- and v-axes, γ is the skew factor, and (u_0, v_0) is the principle point.

The multiview system also involves the use of a projector. In fact, the projector shares the same pinhole model with the camera because it has the inverse optics of a camera (the projector projects images instead of capturing images). Consequently, we can build triangulation between the left camera and the projector through two sets of equation from both devices

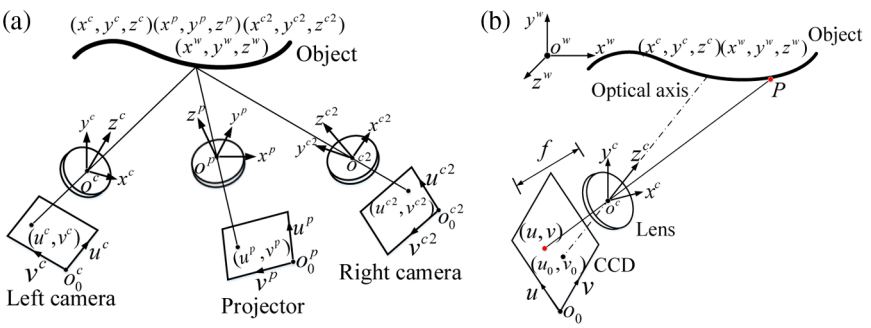

Fig. 3 Right camera candidate projection. (a) Schematic diagram of the multiview system and (b) schematic diagram of the pinhole model.

$$s^c[u^c, v^c, 1]^{\mathrm{T}} = A^c[R^c, t^c][x^w, y^w, z^w, 1]^{\mathrm{T}} = M^c[x^w, y^w, z^w, 1]^{\mathrm{T}}, \tag{7}$$

$$s^p[u^p, v^p, 1]^{\mathrm{T}} = A^p[R^p, t^p][x^w, y^w, z^w, 1]^{\mathrm{T}} = M^p[x^w, y^w, z^w, 1]^{\mathrm{T}}. \tag{8}$$

The superscripts c and p represent the camera and projector parameters, respectively. M^c and M^p are the combination of extrinsic and intrinsic parameters for simplification. In this research, a structured light system calibration method[28] is adopted to obtain all extrinsic matrices $[R^c, t^c]$ and $[R^p, t^p]$ and intrinsic matrices A^c and A^p.

Once the system is calibrated, we can reconstruct the 3-D point for a given left camera pixel (u^c, v^c) and its projector candidate (u^p, v^p). Equations (7) and (8) provide six equations but with seven unknowns. Recall that each projector candidate corresponds to one phase line, which can offer additional phase constraint

$$u^p = f[\Phi(u^c, v^c)]. \tag{9}$$

Simultaneously, solving Eqs. (7)–(9) can uniquely determine the 3-D coordinate (x^w, y^w, z^w) as

$$\begin{bmatrix} x^w \\ y^w \\ z^w \end{bmatrix} = \begin{bmatrix} m^c_{11} - u^c m^c_{31} & m^c_{12} - u^c m^c_{32} & m^c_{13} - u^c m^c_{33} \\ m^c_{21} - u^c m^c_{31} & m^c_{22} - u^c m^c_{32} & m^c_{23} - u^c m^c_{33} \\ m^p_{11} - u^p m^p_{31} & m^p_{12} - u^p m^p_{32} & m^p_{13} - u^p m^p_{33} \end{bmatrix}^{-1} \times \begin{bmatrix} u^c m^c_{34} - m^c_{14} \\ v^c m^c_{34} - m^c_{24} \\ u^p m^p_{34} - m^p_{14} \end{bmatrix}, \tag{10}$$

where m^c_{ij} and m^p_{ij} represent the i'th row and j'th column element in matrices M^c and M^p. The 3-D point is then captured by the right camera. In the same way, if we calibrate the right camera under the same world coordinate system, the projection from 3-D coordinate to right camera imaging plane is ruled by

$$s^{c2}[u^{c2}, v^{c2}, 1]^{\mathrm{T}} = A^{c2}[R^{c2}, t^{c2}][x^w, y^w, z^w, 1]^{\mathrm{T}}. \tag{11}$$

Here, (x^w, y^w, z^w) is the 3-D point to be projected; A^{c2} and $[R^{c2}, t^{c2}]$ denote intrinsic and extrinsic parameters of the right camera; and $[u^{c2}, v^{c2}, 1]$ is the homogeneous coordinate of projected point on the right camera image. We repeat the reconstruction and projection process for all qualified projector candidates as explained in Sec. 2.2. Then, a sequence of right camera candidates is generated on a 2-D imaging plane. Each candidate corresponds to one absolute phase value, and the true correspondence point must be within these candidates. As long as the true correspondence point is selected, we can track it back to find the absolute phase on this pixel.

2.4 *Candidate Rejection and Phase Unwrapping*

For each left camera pixel, we find multiple right camera candidates through the previous steps. Because two candidates have at least a 2π difference on the phase map, they are relatively separated on the image, which makes them easy to be distinguished. A list of criteria below is applied to reject wrong candidates and determine the final corresponding points between two cameras:

- *Mask generation*. We create a mask to separate object from background and apply this mask on both the left and right camera phase maps. Any pixel outside the mask is regarded as invalid. We do not process any invalid pixels on the left camera, and all projected candidates not inside the right camera mask are directly discarded.
- *Volume constraint*. A predefined measurement volume as the system working zone is used in the 3-D reconstruction step. Only 3-D points within the measurement volume will be further projected on the right camera.
- *Relative position consistency*. To produce an unwrapped phase map, we search all left camera pixels by raster scanning. On each line, we scan left camera pixel from left to right. Accordingly, the position of the right camera corresponding point should also change from left to right monotonously without jumping back.

Once the right camera correspondence (u^{c2}, v^{c2}) is uniquely determined, we can trace it back to find the absolute phase value $\Phi(u^{c2}, v^{c2})$ from the projector phase line. Since the projected point may not be an integer pixel, we round it to the final correspondence coordinate and assign the phase value to this integer pixel (x, y)

$$\Phi(x, y) = \Phi(u^{c2}, v^{c2}), \tag{12}$$

$$x = \mathrm{round}(u^{c2}), \tag{13}$$

$$y = \mathrm{round}(v^{c2}). \tag{14}$$

Here, round() denotes an operator that determines the closest integer number. Ideally, the corresponding points from two cameras have exactly the same unwrapped phase, but the practical case is affected by the accuracy of system calibration. Therefore, we calculate the fringe order by a round operator to achieve a π error tolerance

$$k_r(x, y) = \mathrm{round}\left[\frac{\Phi(x, y) - \phi_r(x, y)}{2\pi}\right], \tag{15}$$

where $\Phi(x, y)$ denotes the projector absolute phase, $\phi_r(x, y)$ is the right camera wrapped phase, and $k_r(x, y)$ represents the calculated fringe order. Then, the unwrapped phase $\Phi_r(x, y)$ for the right camera pixel is retrieved by

$$\Phi_r(x, y) = \phi_r(x, y) + 2\pi \times k_r(x, y). \tag{16}$$

3 Experiments

We carried out a series of experiments to verify the performance of the proposed phase unwrapping algorithm. The multiview measurement system consisted of a digital-light-processing projector (model: Dell M115HD) and two complementary metal-oxide-semiconductor cameras (model: point gray Grasshopper3). The projector's resolution was 1280×800 pixels with a 14.95-mm focal length lens having

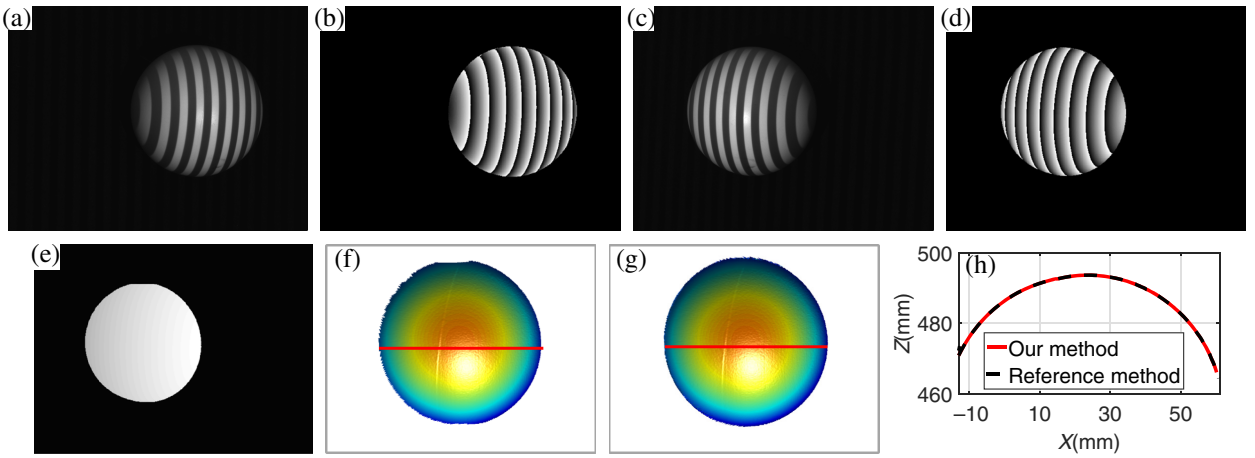

Fig. 4 Experimental results of a uniform sphere from a two camera perspectives (fringe period is 36 pixels). (a) Left camera fringe image; (b) left camera wrapped phase map; (c) right camera fringe image; (d) right camera wrapped phase map; (e) unwrapped phase for right camera using proposed algorithm; (f) 3-D reconstruction by proposed method; (g) 3-D reconstruction by conventional methods; and (h) same cross sections highlighted in (f) and (g).

an aperture of $F/2.0$. Each camera was attached with a pinhole lens (model: Computar M0814-MP2) with a 8-mm focal length, $F/1.4$ aperture, and camera resolution of 640×480 pixels. The system was designed as roughly symmetric: the projector was in the middle, and two cameras were on the two sides with a similar distance to the projector. The calibration volume was $\sim$100 mm $\times$ 140 mm $\times$ 50 mm. The distance between the two cameras was $\sim$265 mm, and the closest distance between projector and object was $\sim$502 mm. The closest distance between the left camera and the object was $\sim$566. Similarly, for the right camera and the object, the closest distance was $\sim$575 mm.

We first measured a smooth sphere with uniform textures. In this experiment, we used 18 steps phase shifted patterns for wrapped phase retrieval. Nearly focused binary patterns with a large step number phase shifting algorithm can achieve high measurement quality.[29] Figures 4(a) and 4(c) show the same fringe pattern captured by the left and right cameras, respectively. Figures 4(b) and 4(d) show the corresponding wrapped phase calculated by the phase shifting algorithm. The distribution of phase changed differently from two camera images because they were observed from different angles, which created unwrapping problems on the boundary of the object. With the implementation of the proposed framework, most of the sphere in the right camera was properly unwrapped, as shown in Fig. 4(e). The 3-D geometry shown in Fig. 4(f) was reconstructed based on the unwrapping result and system calibration. We compared the 3-D result from our algorithm with that from the conventional temporal phase unwrapping using gray-coded binary patterns to determine the fringe order.[7] Note that the conventional method uses seven additional patterns for absolute phase retrieval. The compared results are shown in Fig. 4(g). For better visualization, we took the same cross section from both 3-D results and plotted the depth value curve in Fig. 4(h). The results generated from the proposed phase unwrapping method (blue solid line) perfectly overlaps with the results from the conventional method (red dashed line), proving the success of the proposed method on absolute phase retrieval for a single-object measurement.

Furthermore, we quantitatively analyzed the result obtained from our method and that obtained from the gray-coding method by a quantitative assessment. Figure 5 shows the result. Figure 5(a) shows the difference map, and Fig. 5(b) shows one cross section of the difference map. The mean error of the whole difference map is 1.75×10^{-5} mm and the standard deviation is 3.43×10^{-5} mm, further verifying the success of proposed absolute phase unwrapping algorithm.

A cat statue with a more complex surface geometry was also measured. Figures 6(a) and 6(d) show the texture image from the left and right cameras, respectively, and Figs. 6(b) and 6(e) show the corresponding fringe patterns. Because two cameras observed the statue from different perspectives, some areas can only be captured by one camera, which may cause the failure of correspondence matching. The wrapped phase maps from two cameras are presented in Figs. 6(c) and 6(f). The absolute phase map obtained after employing the proposed phase unwrapping algorithm for the right camera is shown in Fig. 7(a) and the 3-D reconstruction is demonstrated in Fig. 7(b). Similarly, we compared the result obtained from our proposed method and the result obtained from the conventional gray-coding method, shown in

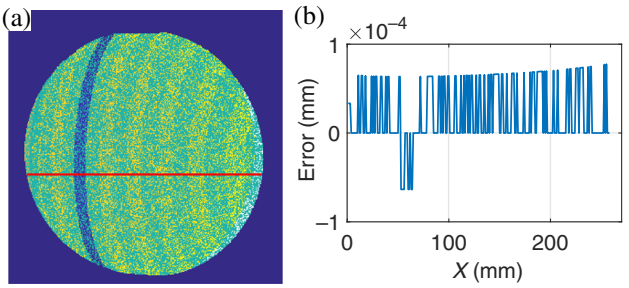

Fig. 5 The measurement error analysis by comparing with the gray-code method. (a) The depth difference map by taking the difference that the measured result obtained from our method and that obtained from the gray-coding method (mean error: 1.75×10^{-5} mm; standard deviation: 3.43×10^{-5} mm) and (b) one cross section of the difference map shown in (a).

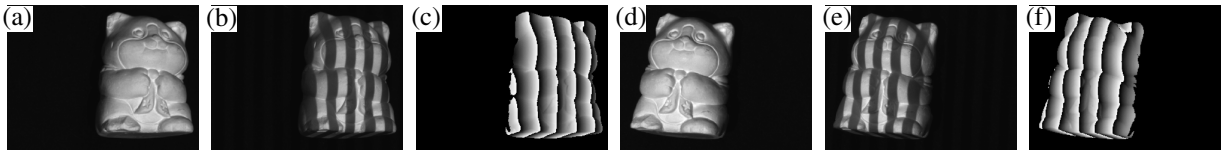

Fig. 6 Experimental results of a cat statue with complex geometry (fringe period is 36 pixels). (a) Left camera texture image; (b) left camera fringe map; (c) 3-D reconstruction by conventional methods; (d) right camera texture image; (e) right camera fringe map; and (f) right camera wrapped phase.

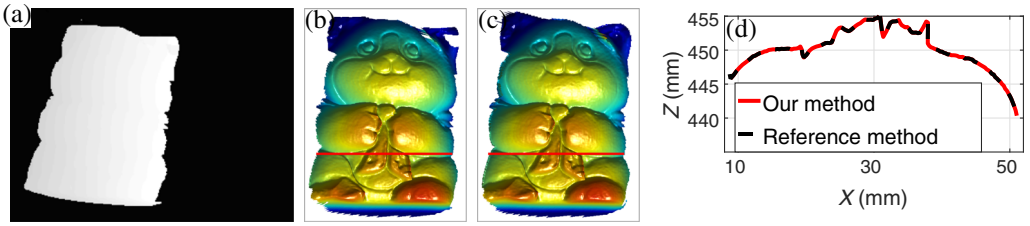

Fig. 7 Comparison between two algorithms. (a) Unwrapped phase for the right camera using the proposed algorithm; (b) 3-D reconstruction by the proposed method; (c) 3-D reconstruction by the conventional method; and (d) same cross sections highlighted in (b) and (c).

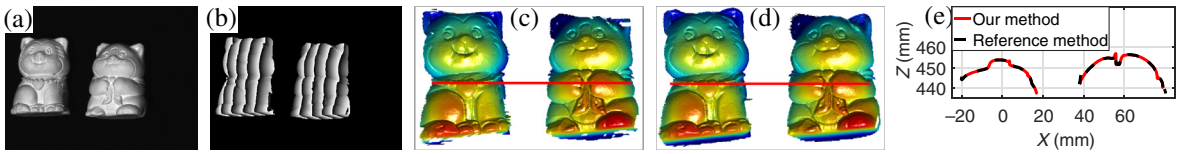

Fig. 8 Experimental results of measuring two isolated objects simultaneously (fringe period is 36 pixels). (a) Right camera texture image; (b) right camera wrapped phase; (c) 3-D reconstruction by proposed method; (d) 3-D reconstruction by conventional methods; and (e) same cross sections highlighted in (c) and (d).

Fig. 7(c). We also took one same cross section of these two 3-D reconstructions; Fig. 7(d) shows the depth curves. The perfect overlap of two curves demonstrates the capability of our proposed algorithm on complex 3-D shape measurement.

Finally, to verify the performance of our method on multiple isolated objects measurements, we simultaneously captured two separate statues. Figure 8 shows the measurement results. The right camera texture image and the wrapped phase map are provided in Figs. 8(a) and 8(b), respectively. From the projector and the left camera pair, the right camera phase was unwrapped by the proposed absolute phase unwrapping framework, from which 3-D geometry was recovered. Figure 8(c) shows the 3-D result. We also employed the conventional temporal phase unwrapping to retrieve the 3-D result, as shown in Fig. 8(d). Again, we took the same cross sections of these two 3-D reconstructions, and Fig. 8(e) shows the perfect overlay of these two depth curves. This experiment along with previous experiment successfully demonstrated that our proposed method can obtain pixel by pixel absolute phase without projecting additional patterns or embedding any features into the phase shifted phase patterns.

4 Summary

This paper presented a multiview geometric constraints-based absolute phase unwrapping framework. Instead of projecting additional patterns, the second camera was added to provide more information for phase unwrapping so that the measurement speed was not affected. We developed the candidate rejection algorithms without backward–forward checks that guarantee a low time cost for correspondence determination. Experimental results proved that the proposed approach can realize absolute phase unwrapping for each pixel; thus, such a method was able to measure both a single object with complex geometry and multiple isolated objects.

Acknowledgments

This study was partially sponsored by the National Science Foundation (NSF) under the Grant No. CMMI-1531048. The views expressed in this paper are those of the authors and not necessarily those of the NSF.

References

1. S. Zhang, "Recent progresses on real-time 3D shape measurement using digital fringe projection techniques," *Opt. Laser Eng.* **48**(2), 149–158 (2010).
2. D. Malacara, *Optical Shop Testing*, 3rd ed., John Wiley and Sons, New York (2007).
3. D. Ghiglia and M. D. Pritt, *Two-Dimensional Phase Unwrapping: Theory, Algorithms, and Software*, Wiley, New York (1998).
4. X. Su and W. Chen, "Reliability-guided phase unwrapping algorithm: a review," *Opt. Laser Eng.* **42**, 245–261 (2004).
5. Y.-Y. Cheng and J. C. Wyant, "Two-wavelength phase shifting interferometry," *Appl. Opt.* **23**(24), 4539–4543 (1984).
6. Y.-Y. Cheng and J. C. Wyant, "Multiple-wavelength phase-shifting interferometry," *Appl. Opt.* **24**(6), 804–807 (1985).
7. G. Sansoni, M. Carocci, and R. Rodella, "Three-dimensional vision based on a combination of gray-code and phase-shift light projection: analysis and compensation of the systematic errors," *Appl. Opt.* **38**(31), 6565–6573 (1999).

8. Y. Li et al., "High-speed and dense three-dimensional surface acquisition using defocused binary patterns for spatially isolated objects," *Opt. Express* **18**, 21628–21635 (2010).
9. S. Zhang, "Composite phase-shifting algorithm for absolute phase measurement," *Opt. Lasers Eng.* **50**(11), 1538–1541 (2012).
10. Z. Zhang, "Microsoft Kinect sensor and its effect," *IEEE Multimedia* **19**(2), 4–10 (2012).
11. A. Wiegmann, H. Wagner, and R. Kowarschik, "Human face measurement by projecting bandlimited random patterns," *Opt. Express* **14**(17), 7692–7698 (2006).
12. L. Zhang et al., "Spacetime faces: high-resolution capture for modeling and animation," in *Data-Driven 3D Facial Animation*, Z. Deng and U. Neumann, Eds., pp. 248–276, Springer, London (2008).
13. W. Jang et al., "Structured-light stereo: comparative analysis and integration of structured-light and active stereo for measuring dynamic shape," *Opt. Lasers Eng.* **51**(11), 1255–1264 (2013).
14. M. Schaffer et al., "Coherent two-beam interference fringe projection for highspeed three-dimensional shape measurements," *Appl. Opt.* **52**(11), 2306–2311 (2013).
15. C. Bräuer-Burchardt et al., "Using geometric constraints to solve the point correspondence problem in fringe projection based 3D measuring systems," in *Int. Conf. on Image Analysis and Processing–ICIAP*, pp. 265–274 (2011).
16. C. Bräuer-Burchardt, P. Kühmstedt, and G. Notni, "Phase unwrapping using geometric constraints for high-speed fringe projection based 3D measurements," *Proc. SPIE* **8789**, 878906 (2013).
17. Y. Huddart et al., "Absolute phase measurement in fringe projection using multiple perspectives," *Opt. Express* **21**(18), 21119–21130 (2013).
18. R. Ishiyama et al., "Absolute phase measurements using geometric constraints between multiple cameras and projectors," *Appl. Opt.* **46**(17), 3528–3538 (2007).
19. Z. Li et al., "Multiview phase shifting: a full-resolution and high-speed 3D measurement framework for arbitrary shape dynamic objects," *Opt. Lett.* **38**(9), 1389–1391 (2013).
20. K. Zhong et al., "Analysis of solving the point correspondence problem by trifocal tensor for real-time phase measurement profilometry," *Proc. SPIE* **8493**, 849311 (2012).
21. K. Zhong et al., "Fast phase measurement profilometry for arbitrary shape objects without phase unwrapping," *Opt. Lasers Eng.* **51**(11), 1213–1222 (2013).
22. K. Kraus, *Photogrammetry: Geometry from Images and Laser Scans*, Walter de Gruyter, Berlin (2007).
23. W. Lohry, V. Chen, and S. Zhang, "Absolute three-dimensional shape measurement using coded fringe patterns without phase unwrapping or projector calibration," *Opt. Express* **22**(2), 1287–1301 (2014).
24. T. Tao et al., "Real-time 3-D shape measurement with composite phase-shifting fringes and multi-view system," *Opt. Express* **24**(18), 20253–20269 (2016).
25. J. E. Greivenkamp, "Generalized data reduction for heterodyne interferometry," *Opt. Eng.* **23**(4), 234350 (1984).
26. R. Hartley and A. Zisserman, *Multiple View Geometry in Computer Vision*, Cambridge University Press, Cambridge (2000).
27. Z. Zhang, "A flexible new technique for camera calibration," *IEEE Trans. Pattern Anal. Mach. Intell.* **22**(11), 1330–1334 (2000).
28. S. Zhang and P. Huang, "Novel method for structured light system calibration," *Opt. Eng.* **45**(8), 083601 (2006).
29. L. Ekstrand and S. Zhang, "Three-dimensional profilometry with nearly focused binary phase-shifting algorithms," *Opt. Lett.* **36**(23), 4518–4520 (2011).

Chufan Jiang is a PhD student working with Dr. Song Zhang at the School of Mechanical Engineering at Purdue University. Her research interests are three-dimensional optical metrology, image processing, and machine learning.

Song Zhang received his PhD from Stony Brook University in 2005. He is an associate professor in mechanical engineering at Purdue University, Indiana, USA. His current research interests include 3-D machine/computer vision, biophotonic imaging, virtual reality, augment vision, human–computer interactions, forensic science, and biomedical engineering. He has authored or coauthored more than 100 research articles. He is the recipient of the NSF CAREER award in 2012 and a fellow of SPIE.